Inorganic Chemistry

Article

From an $S_T = 3$ Single-Molecule Magnet to Diamagnetic Ground State Depending on the Molecular Packing of Mn^{III}salen-type Dimers Decorated by *N,N'*-Dicyano-1,4-naphthoquinonediiminate Radicals

Chihiro Kachi-Terajima,[†] Hitoshi Miyasaka,*,[†,‡] Ken-ichi Sugiura,[†] Rodolphe Clérac,*,[§] and Hiroyuki Nojiri[‡,||]

Department of Chemistry, Graduate School of Science, Tokyo Metropolitan University, 1-1 Minami-ohsawa, Hachioji, Tokyo 192-0397, Japan, CREST, Japan Science and Technology Agency (JST), 4-1-8 Honcho, Kawaguchi, Saitama 332-0012, Japan, Centre de Recherche Paul Pascal, UPR-CNRS 8641, 115 avenue du Dr. A. Schweitzer, 33600 Pessac, France, and Institute for Materials Research, Tohoku University, 2-1-1 Katahira, Sendai 980-8577, Japan

Two manganese(III) tetradentate Schiff-base dimers to which *N,N'*-dicyano-1,4-naphthoquinonediiminate (DCNNQI) radicals are attached have been selectively synthesized by varying the solvents used in the reactions: [Mn$_2$(5-MeOsaltmen)$_2$(DCNNQI)$_2$]·MeOH (**1**) and [Mn$_2$(5-MeOsaltmen)$_2$(DCNNQI)$_2$]·2CH$_2$Cl$_2$·2CH$_3$CN (**2**) [5-MeOsaltmen^{2-} = *N,N'*-(1,1,2,2-tetramethylethylene)bis(5-methoxysalicylideneiminate)]. These two complexes share the same molecular core, [(DCNNQI$^{•-}$)−Mn^{III}−(O)$_2$−Mn^{III}−(DCNNQI$^{•-}$)], where −(O)$_2$− is a biphenolate bridge in the out-of-plane dimerized [Mn$_2$(5-MeOsaltmen)$_2$]$^{2+}$ moiety. However, their packing arrangements are completely different. Whereas complex **1** is found to be relatively isolated, strong intermolecular dimerization of the DCNNQI moieties (with the nearest contact being ∼3.0 Å) is observed in **2**, forming a one-dimensional chain of [−Mn^{III}−(O)$_2$−Mn^{III}−(DCNNQI$^{•-}$)$_2$−]$_\infty$. The magnetic susceptibility of **1** can be modeled with an [$S = 1/2$, 2, 2, $1/2$] four-spin system including strong antiferromagnetic Mn^{III}/DCNNQI radical coupling ($J_{Mn/rad}/k_B = -23$ K) and ferromagnetic Mn^{III}/Mn^{III} coupling through the biphenolate bridge ($J_{Mn/Mn}/k_B = +2.0$ K). These interactions lead to an $S_T = 3$ ground state that possesses significant uniaxial anisotropy ($D_{S=3}/k_B = -2.1$ K). Low-temperature ac and dc magnetic data of **1** reveal its single-molecule magnet behavior with quantum tunneling of the magnetization. By contrast, **2** possesses the diamagnetic ground state induced by dominating Mn^{III}−Mn^{III} antiferromagnetic interactions mediated by the diamagnetic DCNNQI dimers and/or π−π contact along the *b* axis.

Introduction

With the fascination for nanomagnets as the backdrop, the synthesis of paramagnetic polynuclear complexes has motivated chemists who are studying molecular magnetism to discover new superparamagnetic systems at the molecular level, the so-called single-molecule magnets (SMMs).[1] The slow relaxation of the magnetization, which is the most characteristic feature of SMMs, is attributed to the intrinsic property of individual molecules and is governed by the combined effect of uniaxial anisotropy (large negative *D* and small *E*) and the high-spin ground state (S_T). This effect creates an energy barrier (Δ) between the two thermodynamically equivalent spin configurations $m_s = \pm S_T$ that induces a slow reversal of the magnetization from $+S_T$ to $-S_T$ or vice versa. At low temperatures, this characteristic leads to a field-dependent hysteresis phenomenon similar to those observed for classical three-dimensional (3D) ordered magnets. In most of the synthetic strategies used to date, the molecules are prepared in an effort to increase the energy barrier that can be expressed as $\Delta = |D_{ST}|S_T^2$ (for integer spin) or $\Delta = |D_{ST}|(S_T^2 - 1/4)$ (for half-integer spin). Hence, the simplest way to design such molecules is to aggregate anisotropic transition-metal ions in order to increase S_T with

* To whom correspondence should be addressed. E-mail: miyasaka@ agnus.chem.tohoku.ac.jp (H.M.).
† Tokyo Metropolitan University.
‡ CREST-JST.
§ Centre de Recherche Paul Pascal.
|| Tohoku University.

(1) Reviews: (a) Christou, G.; Gatteschi, D.; Hendrickson, D. N.; Sessoli, R. *MRS Bull.* **2000**, *25*, 66. (b) Gatteshi, D.; Sessoli, R. *Angew. Chem.* **2003**, *115*, 278; *Angew. Chem., Int. Ed.* **2003**, *42*, 268.

appropriate intracluster exchange couplings. On the other hand, the minimization of SMM nuclearity is also an important issue. Indeed, such small SMMs offer appealing simple model systems with a small number of quantum energy levels as well as interesting anisotropic building blocks to construct, for example, single-chain magnet (SCM)[2] or multidimensional magnetic materials.[3] Following this approach, we discovered in 2004 the smallest known SMM, which is in a simple out-of-plane dimer of a Mn^{III}salen-type Schiff-base complex possessing an $S_T = 4$ spin ground state: $[Mn_2(saltmen)_2(ReO_4)_2]$ [saltmen^{2-} = N,N'-(1,1,2,2-tetramethylethylene)bis(salicylideneiminate); Chart 1a].[4] Using this type of dinuclear building block together with Ni^{II} coordinating-donor complexes, one-dimensional (1D) assemblies that possess SCM behavior have been synthesized: $[Mn_2(saltmen)_2Ni(pao)_2(L^1)_2](A)_2$ (pao$^-$ = pyridine-2-aldoximate; L^1 = pyridine, 4-picoline, 4-*tert*-butylpyridine, N-methylimidazole; A^- = ClO_4^-, PF_6^-, BF_4^-, ReO_4^-). In these compounds, the slow dynamics of the magnetization is induced by the 1D arrangement of ferromagnetically coupled $[Mn^{III}-Ni^{II}-Mn^{III}]$ units that possess an $S = 3$ spin ground state with strong uniaxial anisotropy. It is worth noting that the key to producing the SCM behavior is the presence of ferromagnetic exchange mediated by the biphenolate bridge in the $[Mn_2(saltmen)_2]^{2+}$ dimeric moiety (Chart 1b).[2c,d] Parallel to these systems, tetranuclear oligomers, $[Mn(5\text{-}Rsaltmen)Ni(pao)(bpy)_2]_2(ClO_4)_4$ [5-Rsaltmen^{2-} = N,N'-(1,1,2,2-tetramethylethylene)bis(5-Rsalicylideneiminate); bpy
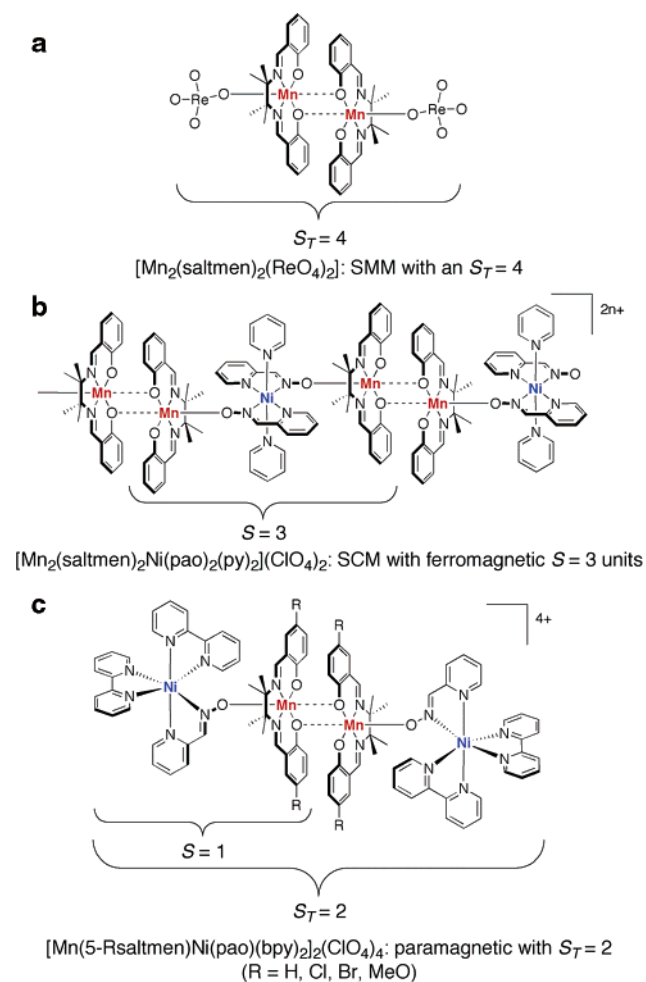
(2) (a) Caneschi, A.; Gatteschi, D.; Lalioti, N.; Sangregorio, C.; Sessoli, R.; Venturi, G.; Vindigni, A.; Rettori, A.; Pini, M. G.; Novak, M. A. *Angew. Chem., Int. Ed.* **2001**, *40*, 1760. (b) Clérac, R.; Miyasaka, H.; Yamashita, M.; Coulon, C. *J. Am.* Chem. Soc. **2002**, *124*, 12837. (c) Miyasaka, H.; Clérac, R.; Mizushima, K.; Sugiura, K.-i.; Yamashita, M.; Wernsdorfer, W.; Coulon, C. *Inorg. Chem.* **2003**, *42*, 8203. (d) Lescouëzec, R.; Vaissermann, J.; Ruiz-Pérez, C.; Lloret, F.; Carrasco, R.; Julve, M.; Verdaguer, M.; Dromzee, Y.; Gatteschi, D.; Wernsdorfer, W. *Angew. Chem., Int. Ed.* **2003**, *42*, 1483. (e) Liu, T.; Fu, D.; Gao, S.; Zhang, Y.; Sun, H.; Su, G.; Liu, Y. *J. Am. Chem. Soc.* **2003**, *125*, 13976. (f) Toma, L. M.; Lescouëzec, R.; Lloret, F.; Julve, M.; Vaissermann, J.; Verdaguer, M. *Chem. Commun.* **2003**, 1850. (g) Pardo, E.; Ruiz-Garcia, R.; Lloret, F.; Faus, J.; Julve, M.; Journaux, Y.; Delgado, F.; Ruiz-Perez, C. *Adv. Mater.* **2004**, *16*, 18, 1597. (h) Chakov, N. E.; Wernsdorfer, W.; Abboud, K. A.; Christou, G. *Inorg. Chem.* **2004**, *43*, 5919. (i) Ferbinteanu, M.; Miyasaka, H.; Wernsdorfer, W.; Nakata, K.; Sugiura, K.; Yamashita, M.; Coulon, C.; Clérac, R. *J. Am. Chem. Soc.* **2005**, *127*, 2090. (j) Kajiwara, T.; Nakano, M.; Kaneko, Y.; Takaishi, S.; Ito, T.; Yamashita, M.; Igashira-Kamiyama, A.; Nojiri, H.; Ono, Y.; Kojima, N. *J. Am. Chem. Soc.* **2005**, *127*, 10150. (k) Bogani, L.; Sangregorio, C.; Sessoli, R.; Gatteschi, D. *Angew. Chem., Int. Ed.* **2005**, *44*, 5817. (l) Sun, Z.-M.; Prosvirin, A. V.; Zhao, H.-H.; Mao, J.-G.; Dunbar, K. R. *J. Appl. Phys.* **2005**, *97*, 10B305. (m) Lecren, L.; Roubeau, O.; Coulon, C.; Li, Y.-G.; Le Goff, X.; Wernsdorfer, W.; Miyasaka, H.; Clérac, R. *J. Am. Chem. Soc.* **2005**, 127, 17353.
(3) (a) Miyasaka, H.; Nakata, K.; Sugiura, K.-i.; Yamashita, M.; Clérac, R. *Angew. Chem., Int. Ed.* **2004**, *43*, 707. (b) Miyasaka, H.; Nakata, K.; Lecren, L.; Coulon, C.; Nakazawa, Y.; Fujisaki, T.; Sugiura, K.-i.; Yamashita, M.; Clérac, R. *J. Am. Chem. Soc.* **2006**, *128*, 3770.
(4) Miyasaka, H.; Clérac, R.; Wernsdorfer, W.; Lecren, L.; Bonhomme, C.; Sugiura, K.-i.; Yamashita, M. *Angew. Chem., Int. Ed.* **2004**, *43*, 2801. Other SMMs having the smallest nuclearity (dinuclear SMM) are [MnCuCl(5-Br-sap)$_2$(MeOH)] (5-Br-sap^{2-} = 5-bromo-2-salicylideneamino-1-propanolate) (by Oshio, H.; Nihei, M.; Yoshida, A.; Nojiri, H.; Nakano, M.; Yamaguchi, A.; Karaki, Y.; Ishimoto, H. *Chem.−Eur. J.* **2005**, *11*, 843. Fujii, Y.; Hayasaki, S.; Hashimoto, H.; Chiba, M.; Yoshida, A.; Nihei, M.; Oshio, H.; Chen, B.; Kubo, T. *Polyhedron* **2005**, 24, 2885) and [Mn$_2$O$_2$(bpy)$_4$](ClO$_4$)$_3$ (by Rajaraman, G.; Sanudo, E. C.; Helliwell, M.; Piligkos, S.; Wernsdorfer, W.; Christou, Brechin, E. K. *Polyhedron* **2005**, *24*, 2450).

Chart 1

a

$S_T = 4$
$[Mn_2(saltmen)_2(ReO_4)_2]$: SMM with an $S_T = 4$

b

$S = 3$
$[Mn_2(saltmen)_2Ni(pao)_2(py)_2](ClO_4)_2$: SCM with ferromagnetic $S = 3$ units

c

$S = 1$
$S_T = 2$
$[Mn(5\text{-}Rsaltmen)Ni(pao)(bpy)_2]_2(ClO_4)_4$: paramagnetic with $S_T = 2$
(R = H, Cl, Br, MeO)

= 2,2′-bipyridine], have been also characterized (Chart 1c). They possess the out-of-plane Mn^{III} dinuclear core decorated by two Ni^{II} complexes. Unfortunately, these $S_T = 2$ complexes do not exhibit SMM properties above 1.8 K.[5] These results demonstrate that the anisotropic out-of-plane $[Mn_2(Rsaltmen)_2]^{2+}$ dimers are interesting building blocks for the design of molecular or 1D assemblies and that their magnetic properties can be tuned according to anisotropy and the spin ground state of the molecule (or unit) containing the $[Mn_2(Rsaltmen)_2]^{2+}$ dimers.

On the basis of these results, one of our research activities has been devoted to the use of $S_T = 4$ Mn^{III}salen-type out-of-plane dimers as the framework to design molecules with a tunable spin state. As shown in the above compounds, the $Ni(pao)_2(L^1)_2$ or $Ni(pao)(bpy)_2$ $S = 1$ metalloligands are attachable to the axial position of the Mn^{III} nuclear core, thereby enabling the spin ground state of assemblies to change according to the exchange couplings between the metal centers; e.g., in the latter tetranuclear complexes, the $S_T = 2$ ground state is induced by the antiferromagnetic $Ni^{II}-Mn^{III}$ interactions via the oximato bridge and the ferromagnetic $Mn^{III}-Mn^{III}$ exchange via the biphenolate bridge. Therefore, replacing the $S = 1$ Ni^{II} metalloligands with an S

(5) Miyasaka, H.; Nezu, T.; Sugimoto, K.; Sugiura, K.-i.; Yamashita, M.; Clérac, R. *Inorg. Chem.* **2004**, *43*, 5486.

$= {}^{1}/_{2}$ organic radical should stabilize $S_T = 3$ complexes according to the expected antiferromagnetic radical/Mn^{III} exchange coupling. Moreover, because of the large uniaxial anisotropy of the Mn^{III} ions, this complex might exhibit SMM behavior. On the basis of the coordination requirements, our choice of the organic radical has led to a family of dicyanoquinodiimine (DCNQI) molecules that allow for strong magnetic interactions between the coordinated metal ions and their radical forms.[6] Herein, the syntheses, X-ray structures, and detailed magnetic properties of two out-of-plane Mn^{III} dimeric compounds decorated by *N,N'*-dicyano-1,4-naphthoquinonediimine (DCNNQI) anions, [Mn$_2$(5-MeOsaltmen)$_2$(DCNNQI)$_2$]·MeOH (**1**) and [Mn$_2$(5-MeOsaltmen)$_2$-(DCNNQI)$_2$]·2CH$_2$Cl$_2$·2CH$_3$CN (**2**) [5-MeOsaltmen^{2-} = *N,N'*-(1,1,2,2-tetramethylethylene)bis(5-methoxysalicylideneiminate)] are reported. Despite the similarity of their molecular structures, these two compounds possess different 3D molecular packing arrangements that induce dramatic changes of their magnetic properties, i.e., SMM behavior for **1** and diamagnetic ground state for **2**.

Experimental Section

General Procedures and Materials. All syntheses were carried out under a N$_2$ atmosphere using standard Schlenk techniques. Solvents were dried with common drying agents and freshly distilled under N$_2$ before use. DCNNQI was synthesized according to the method in the literature.[7] The H$_2$(5-MeOsaltmen) ligand was synthesized by reacting 5-methoxysalicylaldehyde with 1,1,2,2-tetramethylenediamine in a 2:1 molar ratio in a methanol/water mixture.

[Mn^{II}(5-MeOsaltmen)]·nH$_2$O. This compound was prepared using a method similar to the one reported in ref 8. A mixture of Mn(O$_2$CCH$_3$)$_2$·4H$_2$O (0.994 g, 4.1 mmol), H$_2$(5-MeOsaltmen) (1.731 g, 4.5 mmol), and KOH (0.612 g, 10.9 mmol) in 70 mL of methanol was refluxed for 5 h under a N$_2$ atmosphere. The solution was filtered and the filtrate reduced to 10 mL in order to obtain an orange crystalline powder of [Mn^{II}(5-MeOsaltmen)]·nH$_2$O. The sample was collected by suction filtration under a N$_2$ atmosphere, washed with a minimum amount of methanol, and dried in vacuo (yield 1.056 g, 2.3 mmol, 56%). Anal. Calcd for C$_{22}$H$_{26}$MnN$_2$O$_4$·1.4H$_2$O: C, 57.12; H, 6.27; N, 6.06. Found: C, 56.97; H, 5.78; N, 5.93.

[Mn$_2$(5-MeOsaltmen)$_2$(DCNNQI)$_2$]·MeOH (1). A toluene solution (55 mL) of DCNNQI (0.081 g, 0.39 mmol) was added to a methanol solution (20 mL) of [Mn^{II}(5-MeOsaltmen)]·1.4H$_2$O (0.163 g, 0.35 mmol) in a Schlenk flask. The solution was stirred for 2 h and then left undisturbed. Black microcrystals of **1** appeared after approximately 1 h. The crystalline sample was collected by filtration, washed with a minimum amount of dichloromethane (CH$_2$Cl$_2$) and toluene, and dried under a N$_2$ stream (yield: 0.128 g, 0.097 mmol, 55%, based on the Mn ion). Large single crystals of **1** were obtained by slow diffusion of layered solutions of [Mn^{II}-(5-MeOsaltmen)]·1.4H$_2$O (0.163 g, 0.35 mmol) in 25 mL of methanol (top layer) with DCNNQI (0.081 g, 0.39 mmol) in 25

mL of toluene (bottom layer) in a Schlenk tube. X-ray crystallography and magnetic measurements confirmed that these crystals have exactly the same phase as the above polycrystalline sample. Anal. Calcd for C$_{68}$H$_{64}$Mn$_2$N$_{12}$O$_8$·CH$_3$OH: C, 62.82; H, 5.20; N, 12.74. Found: C, 62.62; H, 5.21; N, 12.66. IR (cm^{-1}, KBr): ν-(C≡N) 2122, 2098, ν(C=N) 1601.

[Mn$_2$(5-MeOsaltmen)$_2$(DCNNQI)$_2$]·2CH$_2$Cl$_2$·2CH$_3$CN (2). Compound **2** was obtained as black crystals by slow diffusion in a Schlenk tube of layered solutions of [Mn^{II}(5-MeOsaltmen)]·1.4H$_2$O (0.094 g, 0.20 mmol) in 15 mL of acetonitrile (top layer) with DCNNQI (0.040 g, 0.19 mmol) in 15 mL of CH$_2$Cl$_2$ (bottom layer). The crystals were collected by suction filtration, washed with a minimum amount of CH$_2$Cl$_2$ followed by toluene, and dried under a N$_2$ stream (yield: 0.115 g, 0.075 mmol, 75%, based on the Mn ion). Because compound **2** partially loses its crystallization solvent, CH$_2$Cl$_2$, even at room temperature, the sample used for magnetic measurements was prepared and removed from the mother liquor immediately before measurements. The loss of CH$_2$Cl$_2$ molecules was evaluated to be less than 10% by elemental analysis (vide infra). The crystallization solvents (two CH$_2$Cl$_2$ and two MeCN molecules) were removed in two successive steps with increasing temperature from 20 to 77.6 °C in the first step and from 77.6 to 170.5 °C in the second step, with a total mass loss of 14% (calcd 16.4%). Anal. Calcd for C$_{68}$H$_{64}$Mn$_2$N$_{12}$O$_8$·2CH$_3$CN·1.8CH$_2$Cl$_2$: C, 58.23; H, 4.87; N, 12.88. Found: C, 58.17; H, 5.05; N, 12.83. IR (cm^{-1}, KBr): ν(C≡N) 2122, ν(C=N) 1601.

Physical Measurements. IR spectra were measured on KBr disks with a Shimadzu FT-IR-8600 spectrophotometer. Thermogravimetric and differential thermal analyses were carried out using a Rigaku Thermo Plus TG-8120 apparatus at a heating rate of 5 °C·min^{-1} in flowing dried N$_2$. Cyclic voltammetry (CV) was performed with an ALS/Chi model 600A electrochemical analyzer. Cyclic voltammograms were recorded in CH$_2$Cl$_2$ solutions containing 0.1 M [n-Bu$_4$N](ClO$_4$) as the supporting electrolyte at a scan rate of 0.1 V·s^{-1} at room temperature under N$_2$. A glassy-carbon working electrode, a Pt counter electrode, and an Ag/Ag(NO$_3$) reference electrode were used. The CV potentials were justified by using the ferrocene/ferrocenium couple as an internal reference (Fc/Fc$^+$ = +0.10 V in CH$_2$Cl$_2$ vs Ag/Ag$^+$). Magnetic susceptibilities in the temperature range of 1.8−300 K were measured with a Quantum Design SQUID magnetometer MPMS-XL; dc measurements were conducted from +70 to −70 kOe; ac measurements were performed at frequencies ranging from 1 to 1488 Hz with an ac field amplitude of 3 Oe and no dc applied field. Field dependences of the magnetization at 0.4 and 1.5 K were measured by an inductive method with a ^{3}He refrigerator, where a single-shot pulsed field of up to 20 T was generated with a capacitor bank of 90 kJ. Measurements were performed systematically on finely ground polycrystalline samples that were restrained with n-eicosane or Nujol. Experimental data were corrected for the sample holder and for the diamagnetic contribution calculated from Pascal constants.[9]

Crystallography. Single crystals of **1** and **2** were prepared by the methods described in the synthetic procedure. Single crystals with dimensions of 0.15 × 0.10 × 0.10 mm^3 for **1** and 0.20 × 0.20 × 0.10 mm^3 for **2** were mounted on a glass rod. Data were collected with a Rigaku CCD diffractometer (Saturn 70) with graphite-monochromated Mo Kα radiation (λ = 0.710 70 Å). The structures were solved by heavy-atom Patterson methods (PATTY)[10] and expanded using Fourier techniques (DIRDIF99).[11] Non-

(6) Sugiura, K.-i.; Mikami, S.; Johnson, M. T.; Raebiger, J. W.; Miller, J. S.; Iwasaki, K.; Okada, Y.; Hino, S.; Sakata, Y. *J. Mater. Chem.* **2001**, *11*, 2152.

(7) Aumüller, A.; Hünig, S. *Angew. Chem., Int. Ed. Engl.* **1984**, *23*, 447.

(8) (a) Lewis, J.; Mabbs, F. E.; Weigold, H. *J. Chem. Soc. A* **1968**, 1699. (b) Kessel, S. L.; Emberson, R. M.; Debrunner, P. G.; Hendrickson, D. N. *Inorg. Chem.* **1980**, *19*, 1170. (c) Srinivasan, K.; Michaud, P.; Kochi, J. K. *J. Am. Chem. Soc.* **1986**, *108*, 2309.

(9) Boudreaux, E. A.; Mulay, L. N. *Theory and Applications of Molecular Paramagnetism*; John Wiley and Sons: New York, 1976; pp 491−495.
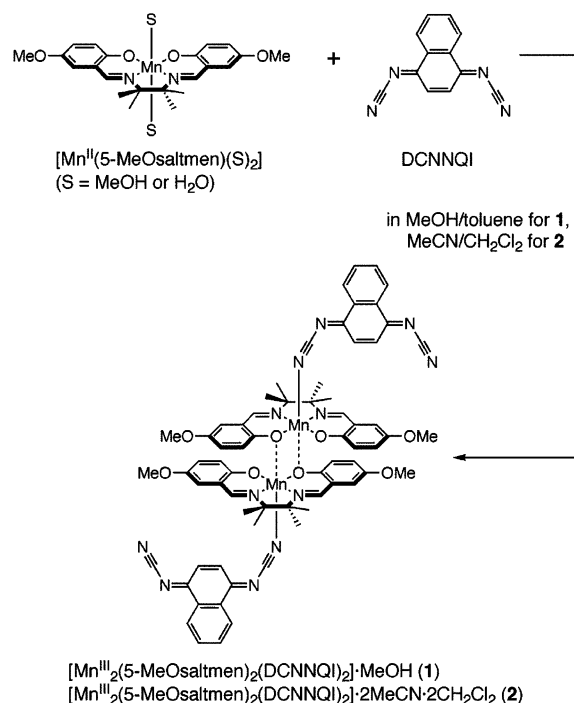
hydrogen atoms were refined anisotropically, whereas hydrogen atoms were introduced as fixed contributors. Full-matrix least-squares refinements on F^2 were based on 5171 and 5864 unique reflections and 453 and 461 variable parameters for **1** and **2**, respectively, and converged with unweighted and weighted agreement factors of $R1 = \sum||F_o| - |F_c||/\sum|F_o| \ [I > 2.00\sigma(I)]$ and $wR2 = [\sum w(F_o^2 - F_c^2)^2/\sum w(F_o^2)^2]^{1/2}$ (all data). A Sheldrick weighting scheme was used. Neutral atom-scattering factors were taken from Cromer and Waber.[12] Anomalous dispersion effects were included in F_{calcd}; $\Delta f'$ and $\Delta f''$ were from Creagh and McAuley.[13] The mass attenuation coefficients were from Creagh and Hubbell.[14] All calculations were performed using the *CrystalStructure* crystallographic software package,[15] and final refinement of **2** was performed using *SHELXL-97*.[16]

Crystal data for 1: $C_{69}H_{68}N_{12}O_9Mn_2$, fw = 1319.25, triclinic, $P\bar{1}$ (No. 2), $T = 103 \pm 1$ K, λ(Mo Kα) = 0.710 70 Å, $a = 8.107$-(6) Å, $b = 14.232(10)$ Å, $c = 14.612(9)$ Å, $\alpha = 71.95(3)°$, $\beta = 68.98(3)°$, $\gamma = 83.82(4)°$, $V = 1496.3(17)$ Å^3, $Z = 1$, $D_{calc} = 1.46$ g·cm^{-3}, $F_{000} = 688.00$, $2\theta_{max} = 61.9°$. Final R1 = 0.065, wR2 = 0.199, GOF = 1.00 for 453 parameters and a total of 14 200 reflections, 7850 unique ($R_{int} = 0.084$). The linear absorption coefficient, μ, for Mo Kα radiation is 4.95 cm^{-1}. Empirical absorption correction was applied, which resulted in transmission factors ranging from 0.8819 to 1.0000. The data were corrected for Lorentz and polarization effects. Maximum positive and negative peaks in the ΔF map were $\rho_{max} = 1.18$ e·Å^{-3} and $\rho_{min} = -1.11$ e·Å^{-3}.

Crystal data for 2: $C_{74}H_{74}N_{14}O_8Mn_2Cl_4$, fw = 1539.18, triclinic, $P\bar{1}$ (No. 2), $T = 103 \pm 1$ K, λ(Mo Kα) = 0.710 70 Å, $a = 10.230$-(5) Å, $b = 12.785(6)$ Å, $c = 14.657(7)$ Å, $\alpha = 76.04(2)°$, $\beta = 73.41(2)°$, $\gamma = 70.16(1)°$, $V = 1705.8(14)$ Å^3, $Z = 1$, $D_{calc} = 1.498$ g·cm^{-3}, $F_{000} = 798.00$, $2\theta_{max} = 62.1°$. Final R1 = 0.088, wR2 = 0.276, GOF = 1.096 for 461 parameters and a total of 15 826 reflections, 8829 unique ($R_{int} = 0.029$). The linear absorption coefficient, μ, for Mo Kα radiation is 5.97 cm^{-1}. Empirical absorption correction was applied, which resulted in transmission factors ranging from 0.9192 to 1.0000. The data were corrected for Lorentz and polarization effects. Maximum positive and negative peaks in the ΔF map were $\rho_{max} = 2.20$ e·Å^{-3} and $\rho_{min} = -1.76$ e·Å^{-3}.

Crystallographic data in CIF format for **1** and **2** are deposited at the Cambridge Crystallographic Data Centre as supplementary publication Nos. CCDC 288928 for **1** and CCDC 288929 for **2**. Copies of the data can be obtained free of charge upon application to CCDC, 12 Union Road, Cambridge CB2 1EZ, U.K. [fax (+44) 1223-336-033; e-mail deposit@ccdc.cam.ac.uk].

(10) PATTY: Beurskens, P. T.; Admiraal, G.; Beurskens, G.; Bosman, W. P.; Garcia-Granda, S.; Gould, R. O.; Smits, J. M. M.; Smykalla, C. *The DIRDIF program system*; Technical Report of the Crystallography Laboratory; University of Nijmegen: Nijmegen, The Netherlands, 1992.

(11) DIRDIF99: Beurskens, P. T.; Admiraal, G.; Beurskens, G.; Bosman, W. P.; de Gelder, R.; Israel, R.; Smits, J. M. M. *The DIRDIF-99 program system*; Technical Report of the Crystallography Laboratory; University of Nijmegen: Nijmegen, The Netherlands, 1999.

(12) Cromer, D. T.; Waber, J. T. *International Tables for Crystallography*; The Kynoch Press: Birmingham, England, 1974; Vol. IV, Table 2.2A.

(13) Creagh, D. C.; McAuley, W. J. In *International Tables for Crystallography*; Wilson, A. J. C., Ed.; Kluwer Academic Publishers: Boston, 1992; Vol. C, Table 4.2.6.8, pp 219−222.

(14) Creagh, D. C.; Hubbell, J. H. In *International Tables for Crystallography*; Wilson, A. J. C., Ed.; Kluwer Academic Publishers: Boston, 1992; Vol C, Table 4.2.4.3, pp 200−206.

(15) *CrystalStructure 3.15: Crystal Structure Analysis Package*; Rigaku and Rigaku/MSC9009: The Woodlands, TX, 2000−2002.

(16) Sheldrick, G. M. *SHELX97*; University of Gottingen: Gottingen, Germany, 1997.

Scheme 1

[Mn^{II}(5-MeOsaltmen)(S)$_2$]
(S = MeOH or H$_2$O)

DCNNQI

in MeOH/toluene for **1**, MeCN/CH$_2$Cl$_2$ for **2**

[Mn^{III}$_2$(5-MeOsaltmen)$_2$(DCNNQI)$_2$]·MeOH (**1**)
[Mn^{III}$_2$(5-MeOsaltmen)$_2$(DCNNQI)$_2$]·2MeCN·2CH$_2$Cl$_2$ (**2**)

Results and Discussion

Synthesis and IR Spectroscopy. Compounds **1** and **2** were synthesized by the redox reaction between neutral starting materials of [Mn^{II}(5-MeOsaltmen)] and DCNNQI. In general, Mn^{II} salen-type Schiff-base compounds are easily oxidized under aerobic conditions to form the corresponding Mn^{III} species; for [Mn^{II}(5-MeOsaltmen)], the oxidation potential is located at $E_{1/2} = -0.34$ V vs Ag/AgNO$_3$ in CH$_2$Cl$_2$. On the other hand, DCNNQI is one-electron-reduced at $E_{1/2} = -0.36$ V vs Ag/AgNO$_3$ in CH$_2$Cl$_2$.[17] The redox reaction of [Mn^{II}(5-MeOsaltmen)]/DCNNQI was carried out under a N$_2$ atmosphere to give a 1:1 stoichiometric complex of Mn(5-MeOsaltmen)/DCNNQI independent of the reaction solvents used, namely, MeOH/toluene for **1** and MeCN/CH$_2$Cl$_2$ for **2** (Scheme 1). Both compounds were isolated as dark-brown crystals. The color of the isolated compounds is in accord with chromophores of Mn^{III} Schiff-base species and the radical form of DCNNQI. The IR spectra of these compounds gave good information on their ionicity and the coordination mode of the DCNNQI moiety in the final product. Both **1** and **2** revealed a ν(C≡N) stretch at 2122 cm^{-1}, which was significantly shifted to shorter wavelength than that of free neutral DCNNQI (2169 cm^{-1}). For coordinated neutral DCNNQI, for example, in [Rh$_2$(O$_2$CCF$_3$)$_4$(DCNNQI)],[18] the ν(C≡N) stretch was found at an even longer wavelength of 2192 cm^{-1}, as is expected for nitrile ligands involving lone-pair σ donations with weak or no metal-to-ligand back-bonding (i.e., the shift to longer wavelength is due to the coordination effect). Hence, the position of the ν(C≡N) stretch obviously indicates that the

(17) The potential of DCNNQI/DCNNQI$^{•-}$ was reported as $E_{1/2} = -0.38$ V in ref 7.

(18) Miyasaka, H.; Campos-Fernández, C. S.; Galán-Mascarós, J. R.; Dunbar, K. R. *Inorg. Chem.* **2000**, *39*, 5870.
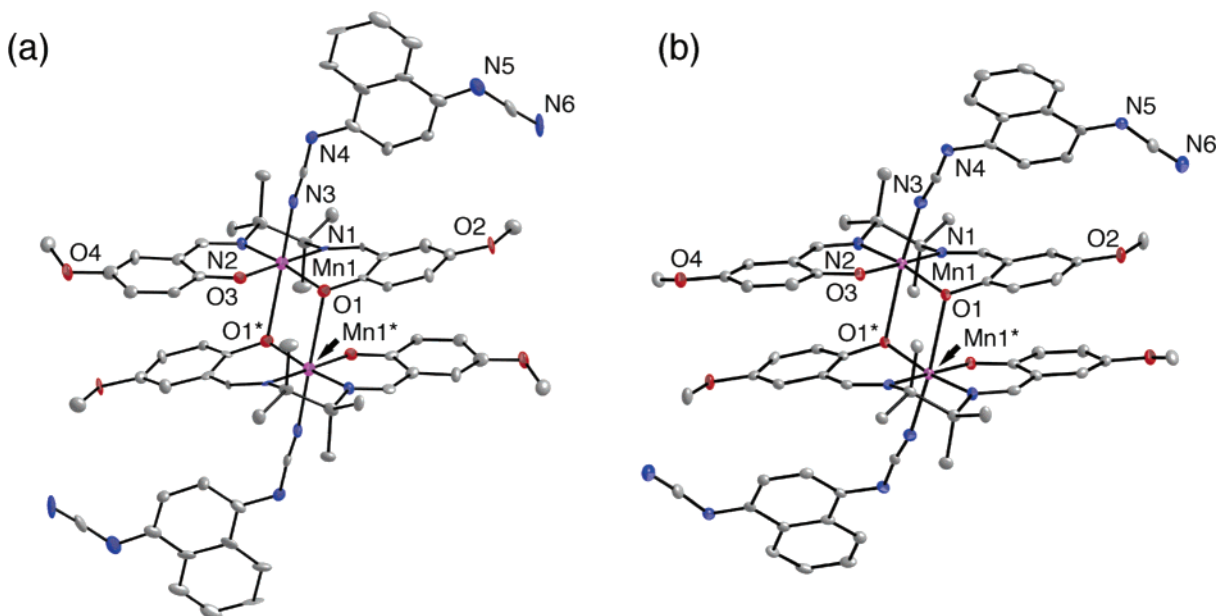
Figure 1. ORTEP drawings of **1** (a) and **2** (b) with thermal ellipsoids set at 50% probability.

DCNNQI moiety in **1** and **2** is reduced to its radical DCNNQI$^{•-}$ form by the redox reaction with [Mn^{II}(5-MeOsaltmen)]. It is interesting to note that a similar shift of the $\nu(C\equiv N)$ band was observed for the series of 2,5-dimethyl-*N*,*N*′-dicyanoquinonediimine (DM-DCNQI): 2188 cm^{-1} for the free neutral DM-DCNQI, 2216 cm^{-1} for the coordinated neutral DM-DCNQI in [Rh$_2$(O$_2$CCF$_3$)$_4$(DM-DCNQI)],[18] 2140 cm^{-1} for the partially reduced form in [TTF][DM-DCNQI] (TTF = tetrathiafulvalene),[19] and 2093 cm^{-1} for the dianionic form in (AsPh$_4$)$_2$DM-DCNQI.[20]

Structural Description. Compounds **1** and **2** were structurally characterized by single-crystal X-ray analysis. Both compounds crystallized in the same triclinic $P\bar{1}$ (No. 2) space group and possessed very similar molecular structures: an out-of-plane [Mn$_2$(5-MeOsaltmen)$_2$] dimer with apical positions occupied by two DCNNQI moieties, as depicted in parts a and b of Figure 1 respectively for **1** and **2**. Nevertheless, the different cell dimensions found for **1** and **2** (see the Experimental Section) are a consequence of the different interstitial solvents (MeOH and 2MeCN·2CH$_2$Cl$_2$ in **1** and **2**, respectively) that induced distinctive packing arrangements (vide infra). Selected bond distances and angles are summarized in Table 1. The centrosymmetrical [Mn$_2$(5-MeO-saltmen)$_2$] moiety in **1** and **2** is similar to that observed in [Mn$_2$(saltmen)$_2$(ReO$_4$)$_2$][4] and its derivatives.[21] In both compounds, each Mn ion is surrounded (i) in its equatorial site by the 5-MeOsaltmen^{2-} ligand with average bond distances of $\langle$Mn$-$N$\rangle_{av}$ = 1.980 and 1.988 Å and $\langle$Mn$-$O$\rangle_{av}$ = 1.887 and 1.882 Å respectively for **1** and **2** and (ii) in the axial positions by nitrogen atoms and oxygen atoms, N3 and O1*,

(19) (a) Aumüller, A.; Peter, E.; Hünig, S.; Meixner, H.; von Schütz, J.-U.; von Schnering, H. G. *Liebigs Ann. Chem.* **1987**, 997. (b) Aumüller, A.; Erk, E.; Hünig, S.; Hädicke, E.; Peter, K.; von Schnering, H. G. *Chem. Ber.* **1991**, *124*, 2001.
(20) Cheruiyot, L. L.; Thompson, L. K.; Greedan, J. E.; Liu, G.; Crutchley, R. J. *Can. J. Chem.* **1995**, *73*, 573.
(21) Miyasaka, H.; Clérac, R.; Ishii, T.; Chang, H.-C.; Kitagawa, S.; Yamashita, M. *J. Chem. Soc., Dalton Trans.* **2002**, 1528.

Table 1. Selected Bond Distances and Angles in Bridging Structures of **1** and **2**
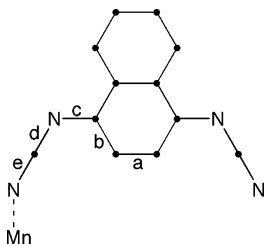
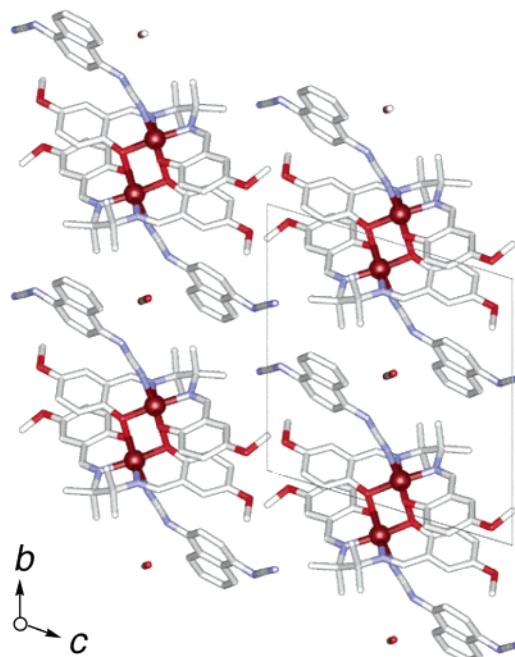|	**1**	**2**
Distance [Å]		
Mn1$-$O1	1.900(4)	1.897(5)
Mn1$-$O3	1.873(4)	1.867(4)
Mn1$-$N1	1.991(5)	1.998(4)
Mn1$-$N2	1.968(5)	1.977(6)
Mn1$-$N3	2.196(7)	2.179(4)
Mn1$-$O1*^{a}	2.633(6)	2.584(4)
Mn1$-$Mn1*^{a}	3.488(2)	3.492(1)
Angle [deg]		
Mn1$-$N3$-$C23	170.5(4)	160.2(6)
O1$-$Mn1$-$O1*^{a}	80.6(2)	78.7(2)
Mn1$-$O1$-$Mn1*^{a}	99.4(2)	101.3(2)

^{a} Symmetry operation (*): $-x, -y, -z + 1$ for **1** and $-x, -y + 1, -z + 1$ for **2**.

from the DCNNQI radical and the neighboring [Mn(5-MeOsaltmen)] moiety, respectively. For the Mn$-$DCNNQI bond, the Mn1$-$N3 bond distance and the Mn1$-$N3$-$C23 bond angle are 2.196(7) Å and 170.5(4)° for **1** and 2.179(4) Å and 160.2(6)° for **2**, respectively. The dihedral angle between the Mn$-$N$_2$O$_2$ equatorial least-squares plane and the DCNNQI least-squares plane is 82.5° for **1** and 62.0° for **2**. For the [Mn$_2$(5-MeOsaltmen)$_2$] unit, the Mn1$-$O1* bond distance and the O1$-$Mn1$-$O1* and Mn1$-$O1$-$Mn1* bond angles are respectively 2.633(6) Å, 80.6(2)°, and 99.4-(2)° for **1** and 2.584(4) Å, 78.7(2)°, and 101.3(2)° for **2** (symmetry operation: *, $-x, -y, -z + 1$ for **1** and $-x, -y + 1, -z + 1$ for **2**). The axial bond distances are significantly longer than the equatorial ones, as is expected for a typical Jahn$-$Teller distortion for hexacoordinated Mn^{III} ions.

The IR data on $\nu(C\equiv N)$ stretches and the oxidation state of the Mn sites, which was easily assigned to III+ from the structural analysis, imply that the DCNNQI moiety must be in a monoanionic radical form in both compounds. Detailed analysis of the bond lengths within the DCNNQI moiety confirmed the above speculations. Indeed, DCNNQI bond

Table 2. Important Structural Parameters for **1** and **2** and Reference Compounds Containing DCNQI Groups

compound	ionicity	a	b	c	d	e	T/K	ref
[Rh$_2$(O$_2$CCF$_3$)$_4$(DCNNQI)]	neutral	1.358(4)	[1.429]^a	[1.314]^a	[1.340]^a	[1.247]^a	90	18
[TTF][DCNNQI]	partial	1.351(5)	[1.432]^a	[1.319]^a	[1.336]^a	[1.155]^a	RT	22
1	ionic	1.39(1)	1.422(9)	1.369(9)	1.30(1)	1.16(1)	103	this work
2	ionic	1.369(9)	1.404(8)	1.356(8)	1.307(7)	1.162(7)	103	this work
[TTF][DM-DCNQI]	neutral	1.342(4)	[1.456]^a	1.308(3)	1.340(4)	1.147(4)	RT	19b
[Mo$_2$(O$_2$CCF$_3$)$_4$(DM-DCNQI)]	neutral	1.369(14)	1.440(13)	1.317(11)	1.368(12)	1.146(12)	104	30
[Cu(DM-DCNQI)$_2$]	partial	1.362(2)	[1.438]^a	1.334(2)	1.311(2)	1.1509(2)	100	31
[MnTMesP][DM-DCNQI]	ionic	1.352(5)	[1.432]^a	1.359(5)	1.309(6)	1.163(6)	198	6
[AsPh$_4$]$_2$[DM-DCNNQI]	dianion		1.406(21)	1.408(19)	1.32(3)	1.15(3)	RT	32

^{a} An average value.

distances are known to be strongly influenced by its oxidation state. Table 2 summarizes relevant structural information of the DCNNQI moiety for **1** and **2**, together with previously reported data for several compounds containing DCNQI groups. The imine N···C bond (c) is, by itself, a good indicator of the oxidation state. Its length is 1.369(9) Å for **1** and 1.356(8) Å for **2**. Both values are significantly larger than those observed for the DCNNQI neutral form in [Rh$_2$(O$_2$CCF$_3$)$_4$(DCNNQI)] (1.314 Å)[18] or the partially reduced form in [TTF][DCNNQI] (1.319 Å).[22] Moreover, a comparison of the DCNQI groups revealed that these bond lengths are intermediate between those of neutral and dianionic species. The results further confirmed the monoanionic nature of the DCNNQI moieties, as was already highlighted by the IR data and charge balance considerations.

Despite their sharing of a very similar molecular motif of [DCNNQI−Mn−(O)$_2$−Mn−DCNNQI] (where −(O)$_2$− is the biphenolate bridge), **1** and **2** exhibit dramatically different packing arrangements, as shown in Figures 2 and 3a, respectively. In **1**, each complex is separated from its neighbors by MeOH molecules that occupy the void space. The interdimer shortest Mn···Mn distance is 7.227(2) Å (the a-axis direction). The Jahn−Teller axes of the [Mn$_2$−DCNNQI$_2$] units are all aligned along the a + b direction. It should be noted that no significant intercomplex π−π contact or hydrogen bond was found between neighbors in **1**, although the intermolecular shortest C···C distance between adjacent 5-MeOsaltmen ligands is 3.301(9) Å in C2···C20$^\#$ (symmetry operation: #, −x + 1, −y, −z + 1), forming a quasi-1D chain arrangement along the a axis. In contrast, in **2**, the [Mn$_2$−DCNNQI$_2$] units form a 1D arrangement along the c axis through the π−π stacking of the DCNNQI moieties with a repeating [−Mn−(O)$_2$−Mn−(DCNNQI)$_2$−]$_\infty$. The nearest C···C distance between the DCNNQI radicals is 3.07(1) Å (Figure 3b), leading to a Mn···Mn distance of 13.1591(10) Å via the (DCNNQI)$_2$

(22) Aumüller, A.; Hädicke, E.; Hünig, S.; Schätzle, A.; von Schütz, J.-U. *Angew. Chem., Int. Ed. Engl.* **1984**, *23*, 449.

Figure 2. Crystal packing of **1** projected along the a axis.

moiety. Furthermore, a π−π stacking of the 5-MeOsaltmen phenyl rings [with the nearest C···O distance of 3.209(7) Å; Figure 3c] was also observed between neighboring chains, forming consequently a 2D layer parallel to the bc plane. In the third direction, the layers are well separated by the interstitial MeCN and CH$_2$Cl$_2$ molecules [the nearest intermetal distance is 10.224(1) Å] and no significant weak interaction was found.

Magnetic Properties of 1. As shown in Figure 4, the χT value of 6.1 cm^3·K·mol^{-1} at 300 K decreases with decreasing temperature to a minimum of 4.25 cm^3·K·mol^{-1} at 27 K, increases slightly to 4.37 cm^3·K·mol^{-1} at 11 K, and finally decreases to 2.14 cm^3·K·mol^{-1} at 1.8 K. This magnetic behavior can be rationalized considering the molecular structure of this compound, which is based on a dinuclear core of S = 2 Mn^{III} metal ions decorated by two S = ^{1}/$_2$

a)

Inter-chain π–π interaction

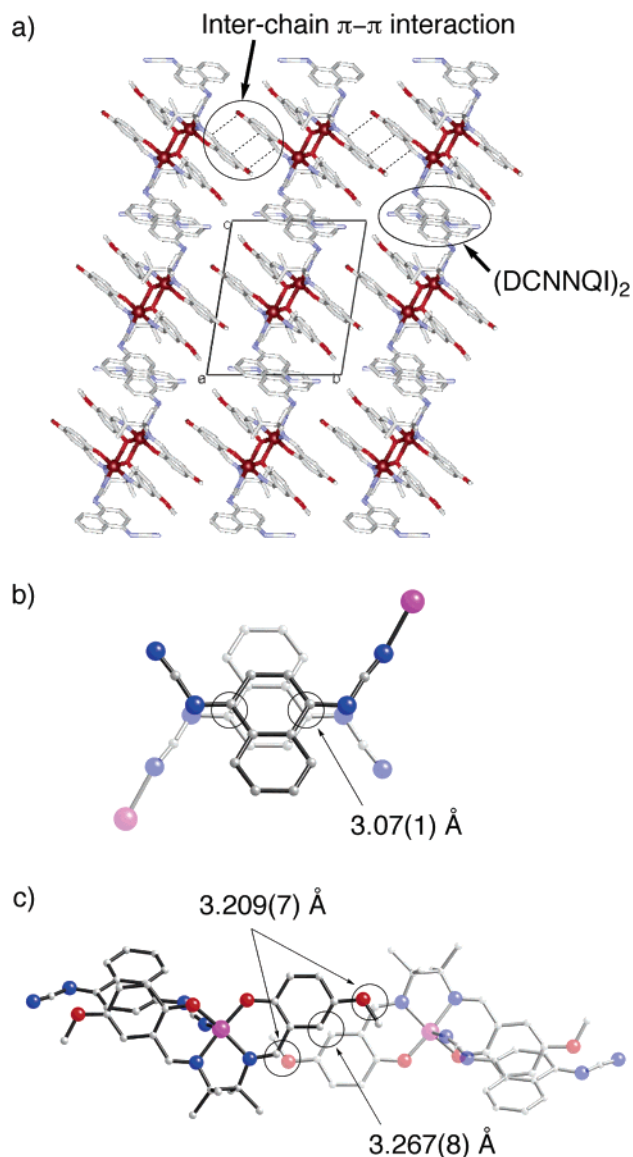(DCNNQI)₂

b)

3.07(1) Å

c)

3.209(7) Å

3.267(8) Å

Figure 3. (a) Crystal packing of **2** projected along the *a* axis. (b) View of the DCNNQI radical overlap by π–π stacking. (c) View of the overlap between [Mn(5-MeOsaltmen)] moieties.

DCNNQI radicals. The magnetic interactions between the two Mn^{III} ions via the biphenolate bridge, $J_{Mn/Mn*}$, and between the Mn^{III} ion and the DCNNQI radical, $J_{Mn/rad}$, are known to lead to weak ferromagnetic and strong antiferromagnetic interactions, respectively.[4,6,21] To estimate these exchange couplings, the magnetic susceptibility of **1** was simulated using, as the first approach, an isotropic Heisenberg spin Hamiltonian for an [$S_{rad} = \frac{1}{2}$, $S_{Mn} = 2$, $S_{Mn} = 2$, $S_{rad} = \frac{1}{2}$] linear tetranuclear model with the following spin Hamiltonian: $H = -2J_{Mn/rad}(S_{Mn}S_{rad} + S_{Mn*}S_{rad*}) - 2J_{Mn/Mn*}(S_{Mn}S_{Mn*})$. To reproduce the final decrease of the χT product, intertetramer interactions (zJ') were considered in the frame of the mean-field approximation (MFA; z is the number of neighboring complexes).[23] From the simulation of the susceptibility using the general procedure developed by Clemente-Juan and co-workers (MAGPACK program),[24] the obtained adequate parameter set is $J_{Mn/rad}/k_B = -23.0(5)$ K, $J_{Mn/Mn*}/k_B = +2.0(1)$ K, $g = 1.95(1)$, and $zJ'/k_B = -0.30(2)$ K (blue line

in Figure 4). It is worth noting that the obtained J values are in good agreement with those estimated in related materials.[4,6,21] Thus, the strong antiferromagnetic exchange between the Mn^{III} ion and the DCNNQI radical and the ferromagnetic exchange via the biphenolate bridge finally lead to an $S_T = 3$ spin ground state for **1** that is almost exclusively populated below 5 K (see the black line in Figure 4, which shows a χT product constant below 5 K). It is important to note that the final decrease of the χT product below 4 K is expected to be not solely due to intertetramer interaction (zJ') but also induced by the magnetic anisotropy (D_{Mn}) of Mn^{III} ions. Therefore, the zJ' value is probably overestimated because it also contains an anisotropic contribution that is impossible to separate on the basis of the χT vs T data. Hence, detailed analysis of the field dependence of the magnetization was performed in order to determine zJ' and D_{Mn} separately. As shown in Figure 5a, the first magnetization curves at 1.8, 1.5, and 0.4 K for **1** saturate to reach 5.85 μ_B at 20 T. The slow saturation of the M vs H data indicates the presence of strong anisotropy in the material that can be roughly estimated from the linear extrapolation of the data between 4 and 7 T at $D_{S=3}/k_B \approx -2.1(1)$ K for **1** with $g = 1.95$ and $S_T = 3$.[25] Returning to the model of the χT vs T data and fixing the $D_{S=3}$ value at -2.1 K (i.e., fixing $\Delta/k_B = 19$ K, as shown on the right-hand side of Figure 4),[26] an excellent simulation is also obtained with the same $J_{Mn/rad}$ and $J_{Mn/Mn*}$ parameters and $D_{Mn}/k_B = -4.3$ K and $zJ'/k_B = -0.23$ K (Figure 4, red line). Note that the g parameters for **1** and **2** (vide infra) obtained from simulating the data with various models lead to g values of 1.93−1.95, which may be slightly low for organic radicals or Mn^{III} metal ions. However, the origin of these low g values is not well understood yet, although it was observed in related materials having the 5-MeOsaltmen^{2-} ligand.[5]

At low fields (below 4 T), several step anomalies are observed on the M vs H curves (Figure 5a), as is expected for SMM complexes when resonant quantum tunneling of the magnetization (QTM) is present.[27] Hysteresis loops measured at 0.4 K and shown in Figure 5b are sweep-field-rate-dependent, and no step in the zero dc field is observed. This last characteristic is the signature of antiferromagnetic interactions between the complexes. Their amplitudes can

(23) To take into account the intercomplex interaction, the following definition of the susceptibility has been used: $\chi = \chi_0/[1 - (2zJ'/Ng^2\mu_B^2)\chi_0]$ where χ_0 is the susceptibility of the noninteracting complexes, z is the number of nearest neighbors, and J' is the magnetic interactions between units. For example, see: (a) Myers, B. E.; Berger, L.; Friedberg, S. *J. Appl. Phys.* **1969**, *40*, 1149. (b) O'Connor, C. J. *Prog. Inorg. Chem.* **1982**, *29*, 203.
(24) Borrás-Almenar, J. J.; Clemente-Juan, J. M.; Coronado, E.; Tsukerblat, B. S. *J. Comput. Chem.* **2001**, *22*, 985.
(25) Minimization of anisotropy and the Zeeman energies gives $2|D_{S=3}|S_T^2 \approx g\mu_B S_T H_a$. Barbara, B.; Thomas, L.; Lionti, F.; Chiorescu, I.; Sulpice, A. *J. Magn. Magn. Mater.* **1999**, *200*, 167.
(26) Note that, in the MAGPACK calculation, this is indeed D_{Mn} that was fixed at −4.3 K. This value was adjusted to obtain an energy gap of 19 K on the $S_T = 3$ ground state (see the right-hand side of Figure 4) that corresponds, as expected, to $D_{S=3}/k_B = -2.1$ K (with $\Delta/k_B = |D_{S=3}|S_T^2$).
(27) (a) Thomas, L.; Lionti, F.; Ballou, R.; Gatteschi, D.; Sessoli, R.; Barbara, B. *Nature* **1996**, *383*, 145. (b) Lecren, L.; Wernsdorfer, W.; Li, Y.-G.; Roubeau, O.; Miyasaka, H.; Clérac, R. *J. Am. Chem. Soc.* **2005**, *127*, 11311.
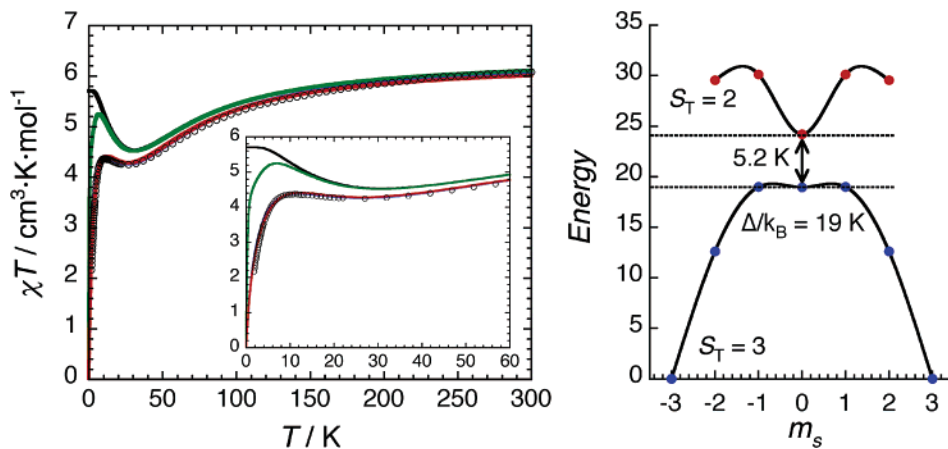
Figure 4. Temperature dependence of the χT product measured on a polycrystalline sample of **1** at 1 kOe. Solid lines are the theoretical results obtained from different models: blue line (superposed to the red line), an isotropic Heisenberg model of four linear $S = \frac{1}{2}, 2, 2, \frac{1}{2}$ spins with intercomplex interactions treated in the MFA ($J_{\text{Mn/rad}}/k_{\text{B}} = -23$ K, $J_{\text{Mn/Mn}*}/k_{\text{B}} = +2$ K, $g = 1.95$, and $zJ''/k_{\text{B}} = -0.3$ K); black line, same as the previous model ("blue model" with the same parameters) but without intercomplex interactions; red line, an anisotropic Heisenberg model of four linear $S = \frac{1}{2}, 2, 2, \frac{1}{2}$ spins with intercomplex interactions treated in the MFA ($J_{\text{Mn/rad}}/k_{\text{B}} = -23$ K, $J_{\text{Mn/Mn}*}/k_{\text{B}} = +2$ K, $g = 1.94$, $D_{\text{Mn}}/k_{\text{B}} = -4.3$ K, and $zJ''/k_{\text{B}} = -0.23$ K); green line, same as the previous model ("red model" with the same parameters) but without intercomplex interactions. On the right: Energy diagram of the two lowest spin states calculated from the fitting of the temperature dependence of the magnetic susceptibility (green model). From $\Delta/k_{\text{B}} = 19$ K, $D_{S=3}/k_{\text{B}}$ can be deduced to be -2.1 K. Note that only the dominant spin contribution for each state was kept to make this figure.
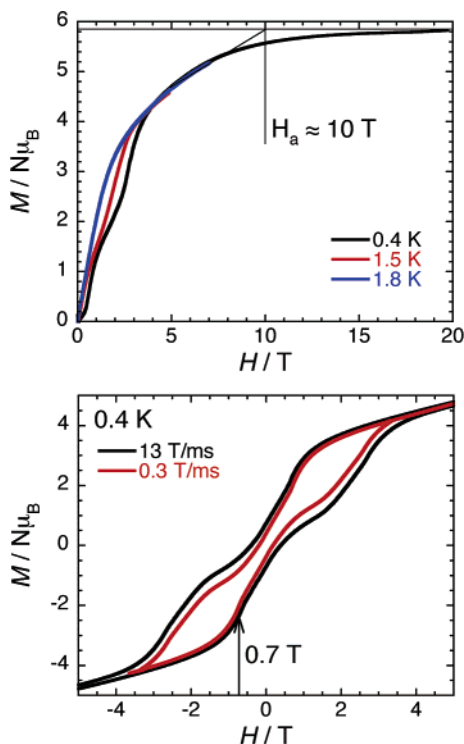

Figure 5. Top: Field dependence of the first magnetization for **1** at 0.4 and 1.5 K using the pulsed-field technique and at 1.8 K with a regular SQUID magnetometer. Bottom: Field hysteresis loops of the magnetization for **1** at 0.4 K using the pulsed-field technique at different sweep-field rates.

be evaluated from the shift of the first step in the field from zero, $H_{\text{ex}} = -0.7$ T, and the following relationship: $g\mu_{\text{B}}H_{\text{ex}}S_{\text{T}} = 2zJ'S_{\text{T}}^2$.[28] Therefore, zJ can be estimated from these data around -0.16 K, in excellent agreement with the above estimation. On the basis of the packing description, this intertetramer antiferromagnetic interaction is probably mediated by the close C···C contact between the 5-MeOsaltmen

(28) Herpin, A. Théorie du magnétisme. *Bibl. des Sciences et Techn. Nucl.*, Presses University de France: 1968.

ligands (~3.3 Å in the *a* axis direction in Figure 2). A more intensive analysis of the step anomalies, which is usually conducted for SMMs when measured on oriented single crystals, is not possible here because of the polycrystalline nature of the sample. Nevertheless, the presence of broad yet well-defined steps indicates without ambiguity the presence of QTM and that **1** possesses SMM behavior with a theoretical energy barrier of $\Delta/k_{\text{B}} = |D_{S=3}|S_{\text{T}}^2 \approx 19$ K (with $S_{\text{T}} = 3$ and $D_{S=3}/k_{\text{B}} \approx -2.1$ K; see the right-hand side of Figure 4). It is interesting to note that a similar behavior was found in the dinuclear complex [Mn$_2$(saltmen)$_2$(ReO$_4$)$_2$] ($S_{\text{T}} = 4$) that displayed SMM properties with $\Delta_{\text{eff}}/k_{\text{B}} = 16$ K (this value was observed in a thermally assisted quantum-tunneling regime; note that in this dimer $D_{S=4}/k_{\text{B}} \approx -1.6$ K and thus $\Delta/k_{\text{B}} = |D_{S=4}|S_{\text{T}}^2/k_{\text{B}} \approx 26$ K).[4] In addition, the ac susceptibility of **1** was measured as a function of temperature (1.8−5 K) and frequency (1−1488 Hz) at the zero dc field with a 3-Oe ac oscillating field (Figure 6). A clear frequency dependence of both χ' and χ'' components was found below 3 K, confirming the conclusions obtained from the dc measurements.

Magnetic Properties of 2. Despite the similarity of their molecular structures, **1** and **2** possess very different magnetic properties (Figures 4 and 7). Above 50 K, the χT product of **2** (Figure 7) is almost constant at approximately 5.65 cm³·K·mol⁻¹, as expected from weakly interacting spin carriers. In this temperature range, the susceptibility obeys the Curie−Weiss law with $C = 5.7$ cm³·K·mol⁻¹ and $\theta = -2.1$ K. Interestingly, the obtained Curie constant corresponds well to the spin-only value of 6.0 cm³·K·mol⁻¹ (for $g = 2.0$) for a set of only two Mn$^{\text{III}}$ ions ($S = 2$). This result is expected because the DCNNQI•⁻ radicals are strongly dimerized as described in the structural part. Such a strong dimerization of radicals usually leads to diamagnetic dimers, as was already reported in the cases of 7,7,8,8-tetracyano-*p*-quinodimethane or tetracyanoethylene radicals.[29] Therefore, in **2**, it appears natural to observe only the magnetism of the
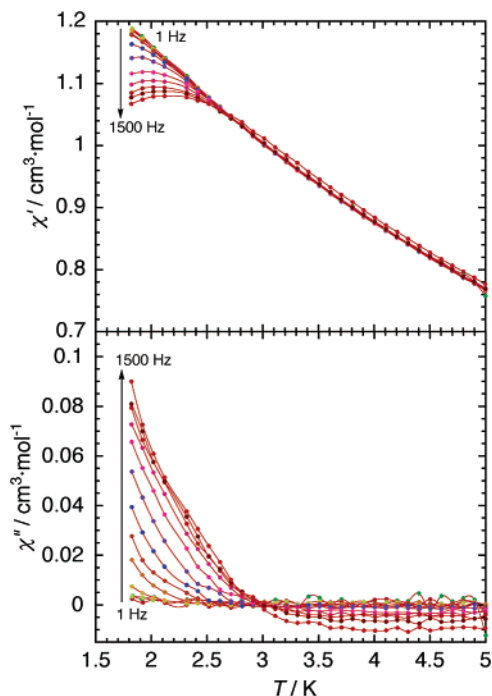
Figure 6. Temperature and frequency dependence of the real (χ') and imaginary (χ'') parts of the ac susceptibility for **1** (zero dc field and 3-Oe ac field). Solid lines are guides for the eyes.
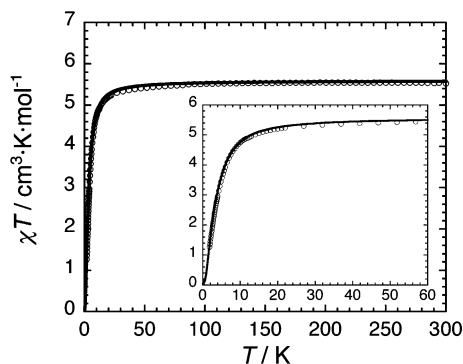

Figure 7. Temperature dependence of the χT product measured on a polycrystalline sample of **2** at 1 kOe. The black line represents a good simulation using an anisotropic Heisenberg dimer model of $S = 2$ with $J'_{Mn/Mn}/k_B = -0.23$ K, $g = 1.94$, and $D_{Mn}/k_B = -4.7$ K.

Mn^{III} spins. It should be underscored that the Mn–Mn interaction via the biphenolate bridge ($J_{Mn/Mn*}$) is expected

(29) For example, see: (a) Ballester, L.; Barral, M. C.; Gutiérrez, A.; Monge, A.; Perpiñán, M. F.; Ruiz-Valero, C.; Sánchez-Pelaez, A. E. *Inorg. Chem.* **1994**, *33*, 2142. (b) Oshio, H.; Ino, E.; Ito, T.; Maeda, Y. *Bull. Chem. Soc. Jpn.* **1995**, *68*, 889. (c) Kunkeler, P. J.; van Koningsbruggen, P. J.; Cornelissen, J. P.; van der Horst, A. N.; van der Kraan, A. M.; Spek, A. L.; Haasnoot, J. G.; Reedijk, J. *J. Am. Chem. Soc.* **1996**, *118*, 2190. (d) Ballester, L.; Gil, A. M.; Gutiérrez, A.; Perpiñán, M. F.; Azcondo, M. T.; Sánchez, A. E.; Amador, U.; Campo, J.; Palacio, F. *Inorg. Chem.* **1997**, *36*, 5291. (e) Ballester, L.; Gutiérrez, A.; Perpiñán, M. F.; Amador, U.; Azcondo, M. T.; Sánchez, A. E.; Bellitto, C. *Inorg. Chem.* **1997**, *36*, 6390. (f) Ballester, L.; Gil, A. M.; Gutiérrez, A.; Perpiñán, M. F.; Azcondo, M. T. *Coord. Chem. Rev.* **1999**, *190–192*, 447. (g) Perpiñán, M. F.; Azcondo, M. T.; Sánchez, A. E.; Coronado, E.; Gómez-García, C. J. *Inorg. Chem.* **2000**, *39*, 2837. (h) Madalan, A. M.; Voronkova, V.; Galeev, R.; Korobchenko, L.; Magull, J.; Roesky, H. W.; Andruh, M. *Eur. J. Inorg. Chem.* **2003**, 1995.

(30) Ouyang, X.; Campana, C.; Dunbar, K. R. *Inorg. Chem.* **1996**, *35*, 7188.

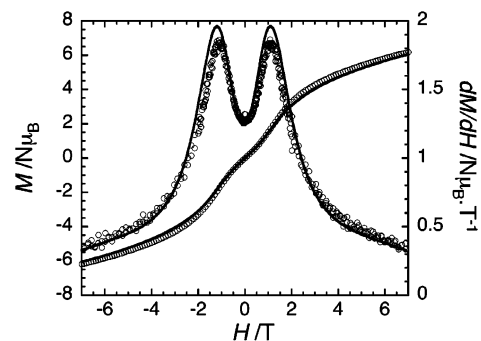(31) Kato, R.; Kobayashi, H.; Kobayashi, A. *J. Am. Chem. Soc.* **1989**, *111*, 5224.

Figure 8. Field dependence of the magnetization and its derivative for **2** at 1.8 K. Black lines represent good simulations using an anisotropic Heisenberg dimer model of $S = 2$ with $J'_{Mn/Mn}/k_B = -0.23$ K, $g = 1.94$, and $D_{Mn}/k_B = -4.7$ K.

to be ferromagnetic, as was observed in **1** and related compounds reported previously.[2b,c,i,4,5,21] Therefore, the decrease of χT below 50 K is certainly associated with two main contributions: (i) magnetic anisotropy (D_{Mn}) arising from Mn^{III} ions and (ii) antiferromagnetic interactions between the Mn^{III} ions probably through the diamagnetic DCNNQI dimers and/or through π–π contact along the b axis (see the Structural Description section). First, the magnetic susceptibility of **2** was fitted to a Mn^{III} dimer model with the following Hamiltonian: $H = -2J_{Mn/Mn*}(S_{Mn}S_{Mn*}) + 2D_{Mn}S_{Mn,z}^2$, where $J_{Mn/Mn*}$ means the interaction via the biphenolate bridge and $S_{Mn,z}$ is the z component of the S_i operators. To take into account the above antiferromagnetic interactions (part ii), the MFA was considered (zJ'), where zJ' includes both types of antiferromagnetic interactions mentioned. From the MAGPACK simulation,[24] the adequate parameters are $J_{Mn/Mn*}/k_B = +0.8(1)$ K, $D_{Mn}/k_B = -4.0(2)$ K, $g = 1.94(1)$, and $zJ'/k_B = -0.50(5)$ K (Figure S1 in the Supporting Information). As expected, the obtained D_{Mn} value is close to the one found for **1**. The Mn···Mn exchange coupling ($J_{Mn/Mn*}$), that is still ferromagnetic, is difficult to estimate exactly from the simulation because its contribution is superposed to the effects of zJ' and D_{Mn} that produce the χT decrease. Moreover, the obtained zJ' value is on the same order of magnitude as $J_{Mn/Mn*}$, and therefore, in the frame of the MFA, the obtained parameters must be treated with caution. Considering that one of the two pathways that mediate antiferromagnetic interaction was dominant, the data were simulated using only a simple Mn^{III} dimer model and considering the following Hamiltonian: $H = -2J'_{Mn/Mn}(S_{Mn}S_{Mn}) + 2D_{Mn}S_{Mn,z}^2$ [where $J'_{Mn/Mn}$ is the interaction through the diamagnetic (DCNNQI)$_2$ bridge]. The χT vs T (at 1000 Oe), M vs H (at 1.8 K), and dM/dH vs H (at 1.8 K) data (Figures 7 and 8) were simultaneously simulated using the MAGPACK program.[24] The adequate parameter set is $g = 1.94(1)$, $J'_{Mn/Mn}/k_B = -0.23(2)$ K, and $D_{Mn}/k_B = -4.7(2)$ K (solid line in Figures 7 and 8). As expected, the obtained D_{Mn} parameter is comparable to the one found for the Mn^{III} ions composing **1** (Figure 4, red line). On the other hand, the magnetic interaction between Mn^{III} ions is antiferromagnetic, illustrating the dominance of the interaction via the

(32) Aquino, M. A. S.; Crutchley, R. J.; Lee, F. L.; Gabe, E. J.; Bensimon, C. *Acta Crystallogr., Sect. C: Cryst. Struct. Commun.* **1993**, *49*, 1543.

(DCNNQI)$_2$ bridge and/or through $\pi-\pi$ contact. Although a remarkably good agreement was found between the experimental data and the simulation (Figures 7 and 8), the amplitude of $J'_{\text{Mn/Ma*}}$ has to be also treated with caution because the $\text{Mn}^{\text{III}}\cdots\text{Mn}^{\text{III}}$ ferromagnetic interaction through the biphenolate bridge was not considered in the model. To summarize, the two simulations clearly indicate that the antiferromagnetic interactions are stronger than, or at least comparable to, the ferromagnetic ones. Hence, **2** exhibits a diamagnetic ground state.

Conclusions

Two Mn^{III}salen-type out-of-plane dimers to which DCN-NQI$^{\bullet-}$ radicals are attached, **1** and **2**, were synthesized by the redox reaction of the Mn^{II} species with the neutral DCNNQI molecule. Both compounds exhibited the same molecular core: $[(\text{DCNNQI}^{\bullet-})-\text{Mn}^{\text{III}}-(\text{O})_2-\text{Mn}^{\text{III}}-(\text{DCN-NQI}^{\bullet-})]$, although different interstitial solvents were present in the void space of the packing (**1**·2MeOH and **2**·2CH$_2$-Cl$_2$·2MeCN). Despite the similarity of their molecular structures, **1** and **2** possessed very different magnetic properties: SMM behavior and diamagnetic ground state, respectively. In **1**, the set of strong antiferromagnetic coupling between the Mn^{III} ion and the DCNNQI$^{\bullet-}$ radical and ferromagnetic coupling between the Mn^{III} sites led to an $S_{\text{T}} = 3$ ground state. As shown by dc and ac magnetic measurements, **1** displayed SMM behavior with QTM at low temperatures. In **2**, the closely packed dimerization of the DCNNQI$^{\bullet-}$ moieties produced the diamagnetic (DCNNQI)$_2$ dimer. As shown by the magnetic measurements, antiferromagnetic interactions between Mn^{III} metal ions, mediated by the diamagnetic DCNNQI dimers and/or $\pi-\pi$ contact along the b axis, dominated the well-known ferromagnetic coupling between the Mn^{III} ions via the biphenolate bridge. Therefore, **2** possessed the diamagnetic ground state. These two compounds illustrate nicely how the variation of the molecular packing arrangement can change dramatically the SMM properties of a given complex.

Supporting Information Available: Crystallographic data in CIF format for **1** and **2** and the χT vs T plot of **2** simulated by the dimer model. This material is available free of charge via the Internet at http://pubs.acs.org.

IC0519842